Catalysis Today 180 (2012) 42–50

Contents lists available at ScienceDirect

Catalysis Today

journal homepage: www.elsevier.com/locate/cattod

Simultaneous water gas shift and methanation reactions on $Ru/Ce_{0.8}Tb_{0.2}O_{2-x}$ based catalysts

José M. Gatica [a,*], Xiaowei Chen [a], Samira Zerrad [a,b], Hilario Vidal [a], Abdelouahid Ben Ali [b]

[a] Departamento C.M., I.M. y Química Inorgánica. Universidad de Cádiz. Puerto Real 11510, Spain
[b] Faculté des Sciences. Université Abdel Malek Essaadi. Rue M'Hannech II, Tétouan 21211, Morocco

ARTICLE INFO

Article history:
Received 31 January 2011
Received in revised form 29 April 2011
Accepted 18 May 2011
Available online 23 June 2011

Keywords:
Ruthenium catalysts
Ceria–terbia mixed oxide
Water gas shift
Methanation
Hydrogen

ABSTRACT

In this paper a $Ru/Ce_{0.8}Tb_{0.2}O_{2-x}/Al_2O_3$ catalyst has been prepared by incipient wetness impregnation method and it has been exhaustively characterized through N_2 physisorption, H_2 and CO chemisorption, temperature programmed desorption, infrared spectroscopy, X-ray diffraction and electron microscopy techniques. The catalyst has been tested in the water gas shift reaction and it has been compared with Ru/Al_2O_3 and $Ru/Ce_{0.8}Tb_{0.2}O_{2-x}$ samples employed as references. This study has revealed that WGS occurs with simultaneous methanation in the ceria–terbia containing systems. Catalytic tests performed in consecutive cycles reveal that the ternary system exhibit higher stability under ageing reaction conditions. These results appear as promising for deep abatement of CO in highly-pure H_2 production from hydrocarbon reforming processes.

1. Introduction

Since many years water gas shift (WGS) reaction has become an important industrial process for hydrogen production, being the usual subsequent key step of methane reforming [1]. In general, inclusion of WGS in end-of-pipe technologies obeys to the fact that it also permits simultaneous abatement of a serious atmospheric pollutant such as carbon monoxide while increasing the amount of hydrogen obtained ($CO + H_2O \rightarrow CO_2 + H_2$). This is particularly critical for fuel cells which require highly pure hydrogen [2]. The demand for this application is so high that an extra preferential oxidation (PROX) and/or methanation unit is normally installed after the WGS reactors to reduce CO to traces, although the latter implies some consumption of the H_2 produced [1,3].

Precisely due to the growing interest for fuel cell development, a lot of literature has been devoted to WGS, in order to establish the basic principles of the reaction, both thermodynamic aspects and kinetics. Nowadays there is no discussion on the exothermic character of the process. On the contrary regarding the mechanism, although many authors support its redox nature, there is still no convergence of idea on the nature of the intermediate, either formate or carboxyl [4]. In any case, it is known that the process is catalyzed, being mixtures of Fe/Cr oxides, and Cu/Zn oxides the catalysts usually employed at high and low temperature respectively [4–6]. In spite of all this, research at lab scale is still open and continuous efforts looking for new formulations with improved performance can be found in literature. In this sense, catalysts containing ceria or ceria–zirconia and one or two transition metals such as Cu, Pd, Pt and Au has recently received great attention [7–12]. In these systems, it has been proposed that ceria can participate both directly mediating in the redox mechanism and facilitating a surface formate intermediate [13].

According to our own experience [14], Ce/Tb mixed oxides exhibit better redox properties than pure ceria, so they might be good candidates for WGS. On the other hand, ruthenium is considered a metal with high activity for methanation ($CO + 3H_2 \rightarrow CH_4 + H_2O$) [15], and additionally it has not been yet commonly used in WGS if compared with other noble metals [16]. Therefore, the purpose of this work has been to investigate a system constituted by a ceria–terbia mixed oxide as promoter and ruthenium as metal phase to evaluate if this formulation is active in WGS and, at the same time, if it is able to abate the unconverted CO via methanation. In this way, these catalysts would operate in a single step what is usually achieved in two. The use of alumina as support has been also considered to enhance the dispersion of both ruthenium and the ceria–terbia mixed oxide. Considering the novelty of the system here investigated particular effort has been accordingly made to characterize the supported phases. A conventional Ru/Al_2O_3 catalyst has been additionally investigated as a reference.

* Corresponding author. Tel.: +34 956 016344; fax: +34 956 016288.
E-mail address: josemanuel.gatica@uca.es (J.M. Gatica).

0920-5861/$ – see front matter © 2011 Elsevier B.V. All rights reserved.
doi:10.1016/j.cattod.2011.05.020

2. Experimental

2.1. Catalysts preparation

The $Ce_{0.8}Tb_{0.2}O_{2-x}/Al_2O_3$ here used as support (hereafter named CT/Al_2O_3) was prepared by co-impregnation of the alumina with a mixture (4:1 Ce/Tb molar ratio) of aqueous solution of $Ce(NO_3)_3{\cdot}7H_2O$ and $Tb(NO_3)_3{\cdot}6H_2O$ by the incipient wetness impregnation technique. The alumina doped with silica (5.72 wt.%) was kindly provided by the GRACE Davison Company. Deposition of the 20 wt.% Ce/Tb mixed oxide was done in one impregnation cycle. The sample was dried overnight at 110 °C and finally calcined in air at 500 °C for 4 h in order to decompose the nitrate precursors.

The target ruthenium catalysts was prepared by impregnation of the cerium–terbium mixed oxide supported on the alumina with an aqueous solution of $Ru(NO)(NO_3)_3$ from 99 wt.% pure ruthenium provided by Alfa Aesar (Johnson-Matthey Company). The noble metal loading obtained after four impregnation/drying cycles was around 3 wt.%. Two reference ruthenium catalysts were prepared using the same incipient wetness impregnation technique and noble metal precursor. For this purpose and in addition to the silica-doped alumina, a $Ce_{0.8}Tb_{0.2}O_{2-x}$ 99 wt.% pure and high surface area mixed oxide (hereafter named CT) from GRACE Davison were used as supports. In all the cases the catalysts precursors were finally reduced in H_2-5% flow at 350 °C (1 h) followed by flushing in He at 400 °C. Before its exposure to the air, ceria containing samples were pulsed with O_2(5%)/He at room temperature (r.t.) to minimize the effects of exothermic reoxidation of the CT oxide. The use of a more conventional oxidative atmosphere for the metal precursor decomposition was avoided in order to prevent the formation of volatile ruthenium tetraoxide that causes losing of the initial metal dispersion [17]. The ruthenium loading (wt.%) of the prepared catalysts was determined by means of inductively coupled plasma (ICP-AES) analysis using an Iris Intrepid instrument (Thermo Elemental) resulting: Ru(2.74%)/$Ce_{0.8}Tb_{0.2}O_{2-x}/Al_2O_3$, Ru(0.67%)/$Ce_{0.8}Tb_{0.2}O_{2-x}$, and Ru(2.84%)/$Al_2O_3$. The lower noble metal loading in the case of the CT mixed oxide support was intentionally chosen in order to maintain similar ruthenium surface density according to the lower surface area of this oxide compared with the alumina-based supports (see Section 3).

2.2. Catalysts characterization

Textural characterization of the catalysts was carried out by N_2 physisorption at −196 °C, using a Micromeritics ASAP 2020. Before the analysis, the samples (aprox. 200 mg) were subjected to heating under high vacuum at 200 °C for 3 h. The isotherms were used to calculate the specific surface area (S_{BET}) and to obtain data related to the micro and meso-porosity of the tested samples.

The H_2 and CO chemisorption studies were conducted in a Micromeritics ASAP 2020C automatic analyzer on samples (aprox. 200 mg) previously reduced *in situ* using H_2-5%/Ar flow at 350 °C (1 h) and subsequently evacuated under high vacuum at 400 °C. The experiments were performed at −20 °C and 35 °C for H_2 analysis, and 30 °C in the case of CO as probe molecule. In the case of sub-ambient temperature the "U" chemisorption quartz reactor was immersed in a Dewar connected to a Haake cooler model EK90. For the CO volumetric adsorption studies, two consecutive isotherms were registered with an intermediate evacuation step (1 h) at the same temperature of the registered isotherms. A range of H_2 or CO pressure of 5–300 Torr was studied and typically 8–11 equilibrium pressure data were acquired. Chemisorption stoichiometries of $H/Ru_S = 1$ and $CO/Ru_S = 1$ were assumed for the metal dispersion estimate.

Temperature programmed desorption of H_2 (TPD-H_2) studies were performed in an experimental device coupled to a Pfeiffer, Thermostar QMS200, quadrupole mass spectrometer using aprox. 150 mg of sample, 60 cm^3/min of He as carrier inert gas and a heating rate of 10 °C/min. The samples were initially reduced at 500 °C with H_2(5%)/Ar flow during 1 h and cooled to r.t. in flowing H_2(5%)/Ar. Quantitative results of these experiences were obtained by means of the mass spectrometer Quadstar 32-Bit software for data acquisition and processing.

The CO interaction with the catalysts was followed by means of FTIR spectroscopy. Spectra were recorded in the transmission mode on a Bruker, Vertex 70, instrument equipped with a DTGS detector. Typically, 100 scans at a resolution of 4 cm^{-1} were averaged. In our study, single self-supported wafers of 13 mm diameter were used. They were prepared by pressing 40 mg of the sample at 5 ton/cm^{-2}. The disk was placed in a transmission infrared quartz cell, with CaF_2 windows, attached to a metallic high-vacuum manifold equipped with a turbo molecular pump (residual pressure <10^{-6} Torr). Previously to the CO adsorption (10 Torr) at r.t., the sample disk was submitted to *in situ* reduction with H_2(5%)/Ar flow at 350 °C during 1 h and evacuation under high vacuum at 400 °C.

X-ray diffraction (XRD) analyses were performed on a Philips PW1820 diffractometer operating with Cu K_α radiation (λ = 1.54 nm) at 40 kV and 40 mA. The 2θ angle ranged from 20° to 120° and the counting step varied from 0.03° to 0.07° depending of the 2θ range. An acquisition time of 6.5 s per point was employed. The ICDD set PDF-2 database JCPDS pattern was used for the phase identification.

High resolution transmission electron microscopy (HRTEM) measurements were performed on a JEOL2010F instrument, with 0.19 nm spatial resolution at Scherzer defocus. High Angel Annular Dark Field-Scanning Transmission Electron Microscopy (HAADF-STEM) images were obtained with the same microscope. An electron probe of 0.5 nm of diameter at a diffraction camera length of 10 cm was used for HAADF mode.

2.3. Activity testing

The catalytic activity tests were performed in a stainless steel reactor using aprox. 100 mg of sample. Before running the reaction the Ru catalysts were reduced at 350 °C (1 h) with H_2(5%)/Ar (60 cm^3/min) and then purged with a He flow at 500 °C for 1 h. The reaction mixture for water gas shift reaction was CO(1%), H_2O(2%) and balance with He. The water content was introduced in the dry gas with a saturator associated with a condenser immersed in a thermostatically controlled bath at to keep the temperature at 17.0 ± 0.1 °C. After the sample pre-treatment, the He flow was shifted to the reaction feed stream (100 cm^3/min) at r.t. and the temperature was raised up to 450 °C at 5 °C/min. The catalytic activity of the sample was also registered in a second temperature ramp (second cycle) after ageing at 450 °C (5 h) and cooling to r.t. under reaction conditions. The profiles of the species of interest were registered using a Pfeiffer, Thermostar QMS200, quadrupole mass spectrometer. The m/e signals obtained were transformed into gas % v/v data by using calibrated CO/He, CO_2/He and CH_4/He mixtures gas cylinders.

3. Results and discussion

3.1. Catalytic activity of Ru catalysts for WGS conditions

Fig. 1 shows the CO conversion as a function of temperature for the ruthenium catalysts. In the case of the Ru/CT catalysts, an initial CO consumption step in the 80–160 °C range should be related to ceria–terbia mixed oxide reduction process as far as only CO_2 production (not H_2 production from WGS activity) is detected. The WGS activity starts from 160 °C reaching 100% CO conversion at

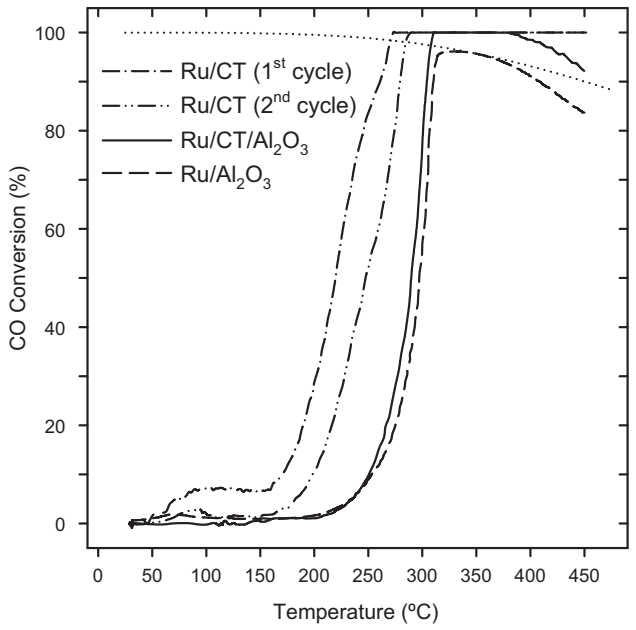

Fig. 1. CO conversion on ruthenium catalysts as a function of temperature. The pre-reduced samples were submitted to the feeding composition CO(1%)/H_2O(2%)/He from r.t. up to 450 °C (first cycle). After ageing during 5 h at 450 °C and cooling at r.t. under the activity test conditions, a second cycle was registered. In the case of the Ru/Al_2O_3 and $Ru/CT/Al_2O_3$ catalysts only the second cycle is showed as far as the results for both cycles are similar. The CO conversion percentage for the thermodynamic equilibrium in the experimental conditions employed is also displayed.

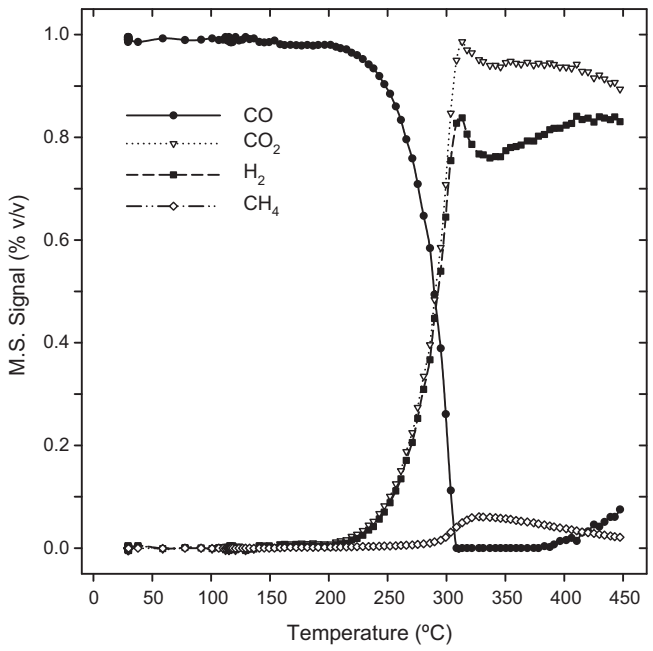

Fig. 2. CO, CO_2, H_2 and CH_4 evolution as a function of temperature during the catalytic test on the $Ru/CT/Al_2O_3$ catalyst previously submitted to ageing at 450 °C (5 h) under the feeding CO(1%)/H_2O(2%)/He composition (second cycle).

274 °C. A relevant effect is that total CO elimination from gas inlet is achieved in the 274–450 °C range exceeding the thermodynamic equilibrium of CO conversion for WGS reaction. From the analysis of the mass spectrometer profiles in which CH_4 is detected besides H_2 and CO_2 we can conclude that both WGS and methanation reactions are occurring in this catalyst. This finding is significant as it indicates that the methanation reaction does not only occur from H_2 as inlet gas [18,19] but it can also take place in an ideal WGS feed stream with an active catalyst for this reaction. Results for the catalyst previously submitted to ageing at 450 °C (5 h) under the feeding 1%-CO/2%-H_2O/He composition make clear a deactivation effect as far as higher temperatures are necessary for 50% and 100% CO conversion (Table 1).

In the case of the Ru/Al_2O_3 catalysts no other products than H_2 and CO_2 are detected obtaining thermodynamic equilibrium of CO conversion for WGS reaction in the 331–370 °C range. The catalytic behaviour of the $Ru/CT/Al_2O_3$ sample remains the same as the one found in the Ru/Al_2O_3 catalysts in relation to their T_{50} temperatures and stability against ageing at 450 °C. Nevertheless simultaneous WGS and methanation reactions also occur in the ternary catalyst. For the $Ru/CT/Al_2O_3$ catalyst, the formation of methane in the 312–387 °C range (Fig. 2) allows the total elimination of CO in the inlet gas. According to the concentration of H_2 and CO_2 in the outlet gas the methanation process shows high selectivity toward CO even at the temperature (328 °C) at which the maximum CH_4 production is measured. This result is significant since the H_2 consumption is maintained low as far as it is mainly limited to the CO unconverted by WGS. Unlike the Ru/CT catalyst, the alumina-containing samples show stability against ageing at 450 °C (5 h) taking into account the similarity between conversion data for the first and second cycles (Table 1). Fig. 3 shows the time on stream for the $Ru/CT/Al_2O_3$ catalyst including the data for the two consecutive cycles (5 h at 450 °C in each) separated in time by a cooling at r.t. in the reaction mixture. The overall results point out the attractive catalytic performance of the ternary system here investigated.

3.2. Textural characterization

Fig. 4 and Table 2 report the results of the textural characterization by means of N_2 physisorption. The registered isotherms (not shown) for all the samples containing alumina are type II with a type H3 hysteresis according to IUPAC definition [20] characteristic of macroporous solids including mesoporosity in some extent. The ceria–terbia mixed oxide and the Ru/CT catalysts feature an isotherm of type IV typically associated with mesoporous solids. Although the surface area for the CT sample is around half the one corresponding to the alumina, its BET value can be considered relatively high for this type of ceria-based oxides. In the case of the $Ru/CT/Al_2O_3$ system, the successive incorporation of ceria–terbia and ruthenium phases induces a noticeable textural modification

Table 1
Results of the water gas shift reaction tests on the ruthenium catalysts.

Catalyst	T_{50} (°C)	$T_{Max.\ CO\ conv}$ (°C) (% Max. CO conversion)[b]	T interval (°C) for 100% CO conversion
Ru/CT, first cycle	219	274 °C (100%)	274–450 °C
Ru/CT, second cycle[a]	247	289 °C (100%)	289–450 °C
Ru/Al_2O_3, first cycle	298	331 °C (96%)	Not reached
Ru/Al_2O_3, second cycle[a]	297	330 °C (96%)	Not reached
$Ru/CT/Al_2O_3$, first cycle	294	312 °C (100%)	312–387 °C
$Ru/CT/Al_2O_3$, second cycle[a]	290	311 °C (100%)	311–388 °C

[a] Sample submitted to a first catalytic test run from r.t. up to 450 °C (5 h) and cooled to r.t. under the reaction gas (1%-CO/2%-H_2O/He).
[b] Minimum temperature for the maximum conversion showed into brackets.

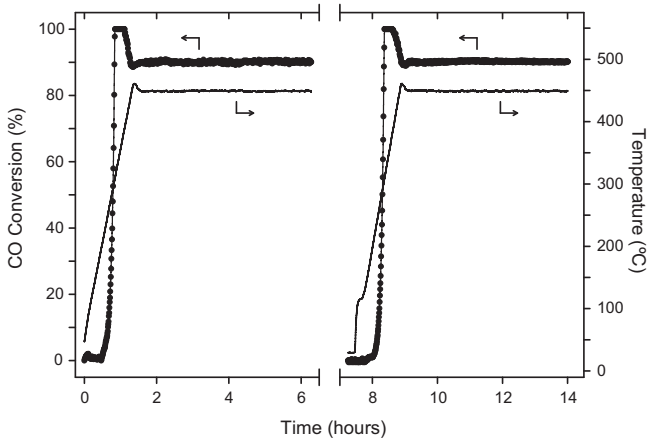

Fig. 3. Time on stream of the $Ru/CT/Al_2O_3$ catalyst submitted to two consecutive cycles including ageing at 450 °C (5 h) in the $CO(1\%)/H_2O(2\%)/He$ reaction mixture. Percentage of CO conversion (•) and temperature (——) data versus time are shown.

Table 2
Textural properties of the samples as determined by N_2 physisorption.

Sample	S_{BET} (m^2/g)	Micropore volume (cm^3/g)[a]	Total pore volume (cm^3/g)[b]
CT	83.3	0.000	0.169
Ru/CT	79.5	0.000	0.162
Al_2O_3	216.2	0.006	0.890
Ru/Al_2O_3	198.5	0.010	0.758
CT/Al_2O_3	175.7	0.005	0.670
$Ru/CT/Al_2O_3$	155.6	0.004	0.570

[a] As estimated by means of *t*-plot analysis.
[b] BJH adsorption cumulative volume of pores.

of the starting alumina. Basically a decrease in BET surface area in parallel to the pore volume data (Table 2) corresponding to pores in the mesoporosity range (Fig. 4) is observed, presumably due to the blockage or partial filling with the supported phases. This effect can be also noticed when the ruthenium is incorporated directly to the alumina in the case of the Ru/Al_2O_3 catalyst. According to *t*-plot diagrams and micropore volume estimate (Table 2) neither Al_2O_3 nor CT mixed oxide alone show significant evidence of microporosity.

3.3. XRD studies

In the case of the $Ru/CT/Al_2O_3$ system, the X-ray diffraction study was focused in obtaining data concerning the structural nature of the supported cerium–terbium mixed oxide. Additionally we looked for evidences of the ruthenium dispersion degree in the Ru-containing samples. Fig. 5 presents the XRD diagrams of the ruthenium catalysts and the CT/Al_2O_3 support. The diffractogram corresponding to the Ru/Al_2O_3 sample mostly displays three distinct reflections at 2θ: 37.6° (3 1 1 reflection indexed according to the *Fd*3*m* space group), 45.9° (4 0 0) and 67.1° (4 4 0), which is in agreement with the database standard an also the powder XRD studies of commercial γ-alumina [21]. The XRD profile of the Ru/CT catalyst clearly indicates the ceria–terbia solid solution presence and corresponds to the cubic fluorite-type lattice. In particular no lines pertaining to terbium oxide are observed which implies that terbia is part of the ceria structure [22]. The XRD diagrams for both $Ru/CT/Al_2O_3$ and CT/Al_2O_3 are very similar indicating that the ruthenium incorporation does not modify the structural nature of the ceria–terbia supported on alumina. In spite of their complexity, these diagrams can be well indexed only considering both the γ-alumina and ceria (CT solid solution) phases. It is important to point out that we can exclude the presence of $LnAlO_3$ (Ln:Ce or Tb) aluminate phase. This finding is expected taking into account the temperatures used for the samples preparation (500 °C at air in the case of the CT/Al_2O_3 support and 350 °C in H_2-5% for the $Ru/CT/Al_2O_3$ catalysts) as far as temperatures higher than 800 °C for the calcination at air and 600 °C in H_2 atmosphere are necessary for $CeAlO_3$ formation in CeO_2/Al_2O_3 samples [23]. From these results we can conclude that the cerium–terbium mixed oxide is dispersed onto the surface of the alumina excluding massive loss of lanthanide effects by means of its incorporation to the alumina or significant migration of aluminium ions to the ceria–terbia solid solution. Estimate of the average crystal size of CT mixed

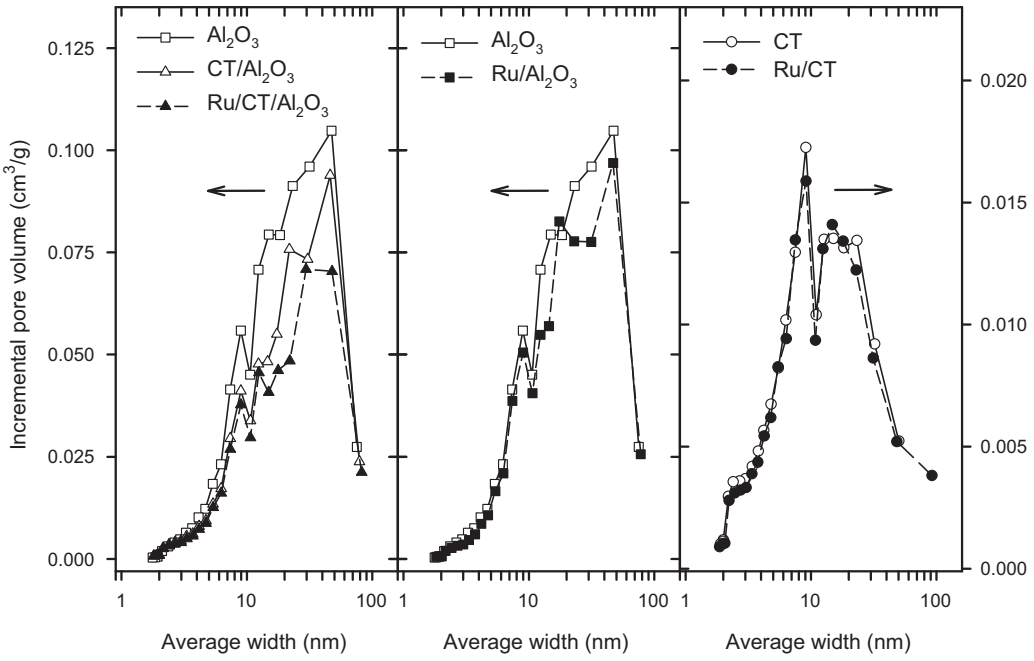

Fig. 4. Pore size distribution curves for ruthenium catalysts and supports. Incremental pore volume graphs from the BJH analysis of the N_2 isotherms adsorption data are shown. Notice the Y-scale change for the Ru/CT and CT samples (right graph).

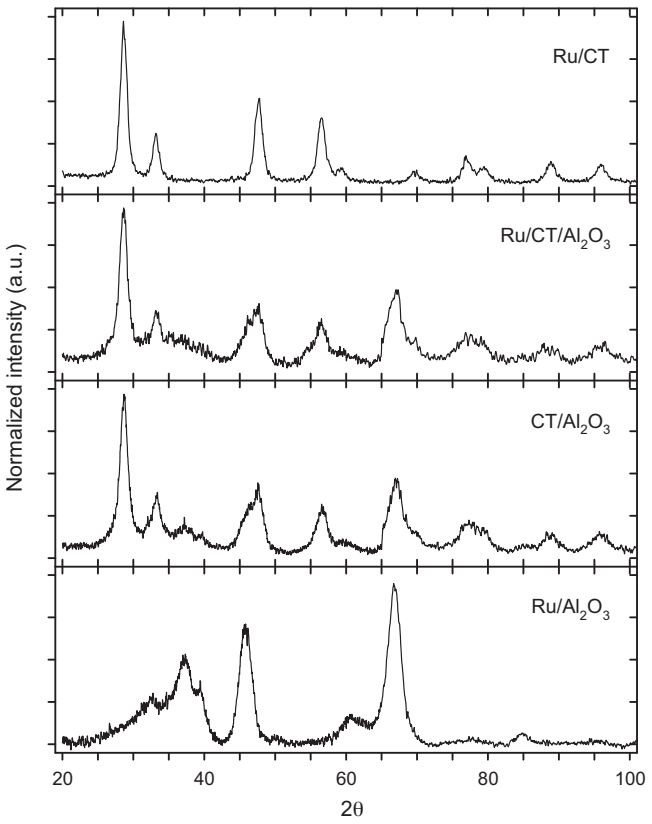

Fig. 5. X-ray diagrams obtained for the ruthenium catalysts and $Ce_{0.8}Tb_{0.2}O_{2-x}$(20 wt.%)/Al_2O_3 support. The figure includes major lines of the JCPDS patterns corresponding to cubic CeO_2 (reference no. 00-034-0394) and cubic γ-Al_2O_3 (00-010-0425). Unequivocal signals corresponding to hexagonal Ru (00-006-0663) and cubic $CeAlO_3$ (00-028-0260) at 2θ: 44.004° and 41.481° respectively, have been not detected in the experimental diffractograms.

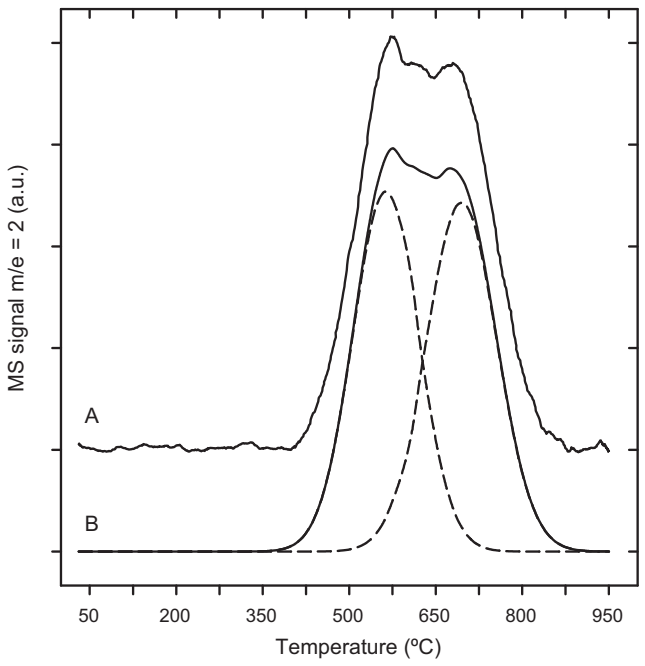

Fig. 6. H_2-TPD trace for the $Ce_{0.8}Tb_{0.2}O_{2-x}$(20 wt.%)/Al_2O_3 support treated with H_2(5%)/Ar at 500 °C (A). In (B) we show the results of the mathematical deconvolution of the experimental H_2 trace including the two gaussian peaks centred at 563 °C (area, 1.51) and 695 °C (area, 1.57) and its combination.

oxide phase was done using the Scherrer equation corrected by Bueno-Ferrer et al. for pure and doped cerium oxides [24] resulting 14.4 nm. Concerning the noble metal phase there is no indication of presence of massive Ru particles in the XRD diffraction diagrams in good agreement with its low loading and the technique used for the preparation of the catalysts. It is most likely that ruthenium is well dispersed on Al_2O_3, CT, and CT/Al_2O_3 supports.

3.4. H_2-TPD results

The methodology developed by Bernal et al. in [25] for $Ce_{0.8}Tb_{0.2}O_{2-x}$/La_2O_3–Al_2O_3 samples have been used to determine the dispersion, i.e., the amount of exposed surface area, of the supported CT in the Ru/CT/Al_2O_3 catalyst. Basically hydrogen chemisorption data obtained from H_2-TPD experiments conducted on samples treated under H_2(5%)/Ar at 500 °C allow to estimate the active surface area of the cerium–terbium mixed oxide. For this purpose we apply the value corresponding to the limit of the capacity to adsorb hydrogen (4.5 atoms of H/nm^2) determined for a pure $Ce_{0.8}Tb_{0.2}O_{2-x}$ treated in the same way and consider that the process is limited to the surface. Fig. 6 shows the H_2-TPD profile obtained for the CT/Al_2O_3 saturated with hydrogen after the above mentioned treatment and subsequent cooling under the same reducing stream from 500 °C up to r.t. The diagram is analogous to those reported in [25] featuring two overlapped peaks with maxima at approx. 550 °C and 700 °C. The possible existence of a third peak between the maxima above indicated can be reasonably excluded from the results of the deconvolution of the H_2 trace (see details in Fig. 6). The quantitative analysis of the experimental TPD trace provides 39.4 μmol H_2/g of sample or 196.5 μmol H_2/g of CT considering its 20 wt.% loading. Taking into account the above indicated limit for hydrogen adsorption on a pure $Ce_{0.8}Tb_{0.2}O_{2-x}$ mixed oxide expressed as 3.74 μmol H_2/m^2 CT, the resulting dispersion is 52.5 m^2/g of mixed oxide. From these results we can estimate the surface area exposed of the ceria–terbia oxide in 10.5 m^2/g of the $Ce_{0.8}Tb_{0.2}O_{2-x}$/La_2O_3–Al_2O_3, thus it is the 6% of the BET surface area of this sample (175.7 m^2/g). Also of interest, assuming a spherical geometry for $Ce_{0.8}Tb_{0.2}O_{2-x}$ crystallites and the density of 7.132 g/cm^3 of pure ceria, the CT crystallite size related to its dispersion can be estimated resulting a 16 nm diameter in good agreement with the data obtained from the XRD study.

3.5. Characterization by means of electron microscopy techniques

Fig. 7 Because the atomic numbers of Ce and Tb are higher than that of aluminium, the brighter part in Fig. 7a is attributed to the $Ce_{0.8}Tb_{0.2}O_{2-x}$ mixed oxide. It can be seen that the ceria–terbia crystals aggregate on alumina support with a diameter between 60 and 100 nm. However, using EDX technique Ce and Tb are also detected in the dark part of the image which is supposed to be alumina (Figure S1 in the Supporting Information). This means that some small crystals of ceria-based phase are dispersed on the alumina support but this cannot be observed easily due to the limitation of detection of Ce and Tb using the HAADF technique. The HRTEM image, representative of the sample, suggests that the crystal size of $Ce_{0.8}Tb_{0.2}O_{2-x}$ is around 15 nm and its structure matches that of ceria, which agrees with the XRD and H_2-TPD results.

A representative HAADF image and the particle size distribution of Ru/CT/Al_2O_3 resulting from measuring the size of over a hundred of ruthenium particles are shown in Fig. 8. HAADF results suggest that Ru is well dispersed on all the surface of the CT/Al_2O_3 support, i.e., Ru is not only dispersed on the islands of $Ce_{0.8}Tb_{0.2}O_{2-x}$ but also on the alumina support. Moreover, taking into account the H_2-TPD and textural results this means that Ru is mainly on the Al_2O_3. The Ru particles are in the range of 1–4 nm. Processing of the particle size distribution and assumption of hexagonal bi-pyramidal

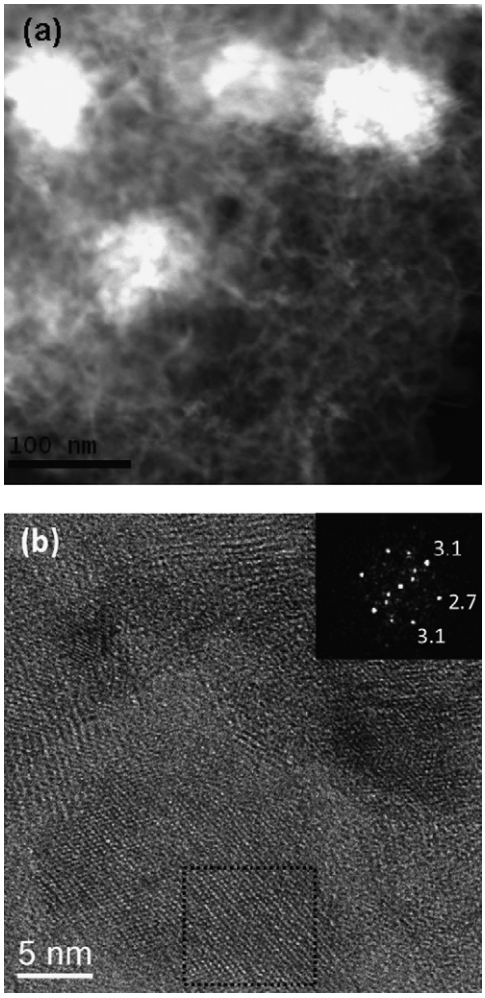

Fig. 7. Representative HAADF image of CT/Al_2O_3 support (a) and HRTEM image of CT/Al_2O_3 support including the digital diffraction pattern of the selected area, which corresponds to Ce–Tb mixed oxide in the [1 1 0] zone axis (b).

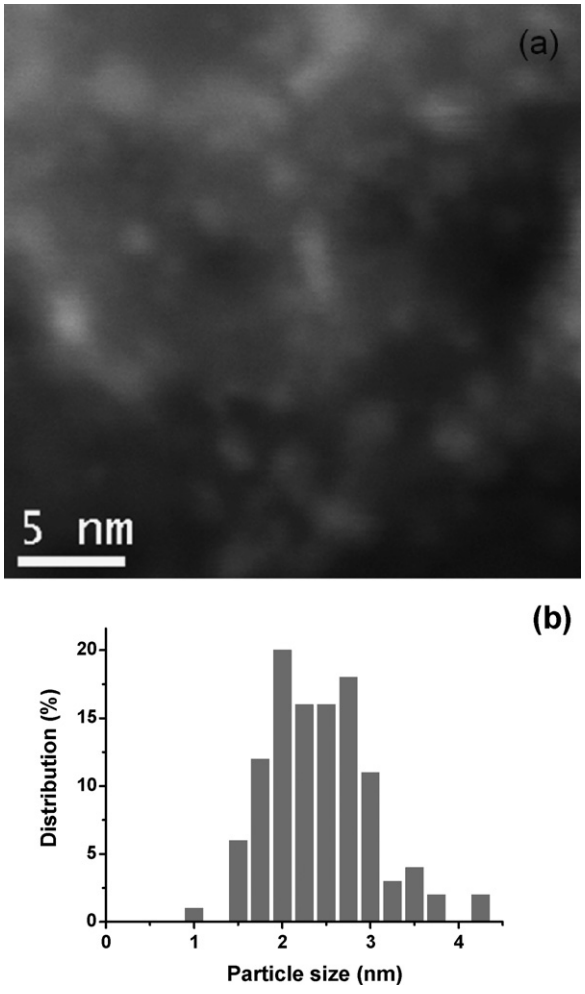

Fig. 8. Representative HAADF image of $Ru/CT/Al_2O_3$ catalyst (a) and ruthenium particle size distribution of $Ru/CT/Al_2O_3$ catalyst (b).

morphology for the metal particles lead to a Ru dispersion around 37%. In the case of Ru/CT catalyst, metal particles cannot be detected which suggests a higher ruthenium dispersion on the CT support.

3.6. H_2 and CO adsorption volumetric studies

Fig. 9 shows the H_2 isotherms registered for the Ru catalysts and Table 3 summarizes the quantitative results of these experiments. According to the amount of H_2 adsorbed at 35 °C (H/Ru = 4.64) intense hydrogen spill-over phenomena in the Ru/CT sample take place. This result points out that ruthenium have an interaction with H_2 similar to other noble metals (Rh, Pt and Pd) when supported onto ceria [26] or ceria-zirconia [27]. The use of sub-ambient temperature in H_2 chemisorption volumetric experiments allows obtaining reliable platinum and rhodium dispersion data in ceria based catalysts [27]. However it is important to notice that references about the activated nature of the H_2–Ru interaction appear from early papers [28] until recently [29]. In this sense, the use of low temperatures could limit kinetically the covering of the exposed ruthenium surfaces rendering under estimations of the metal dispersion. The amount of hydrogen determined for the Ru/CT catalyst at −20 °C can be reasonable related to the metal phase (H/Ru = 0.41) excluding the support. Nevertheless, the profile of the isotherm (Fig. 9) shows the existence of an activated with H_2 pressure effect that suggests a hydrogen adsorption kinetically slow on the metal or the support via spill-over. From these data we cannot obtain reliable data for the ruthenium dispersion in the Ru/CT catalyst.

Although the existence of hydrogen spill-over cannot be discarded only from H_2 isotherm volumetric studies, its intensity would be much less important in the case of the alumina containing catalysts. In this sense, the volumetric data can be used to estimate the metal dispersion in these samples resulting 27–44% ($Ru/CT/Al_2O_3$) and 31–59% (Ru/Al_2O_3), respectively from data obtained at -20 °C and 35 °C in each case. Taking into account the HAADF-STEM results, the use of sub-ambient temperatures in the H_2 adsorption studies could be not adequate in ruthenium catalysts as far as it could lead to low hydrogen surface coverage. Certainly further investigation is necessary in order to optimize

Table 3
Volumetric studies of H_2 chemisorption on the Ru catalysts.

Catalyst	Amount of H_2 adsorbed in cm^3/g STP (H/Ru)[a]	
	−20 °C	35 °C
Ru/CT	0.30 (0.41)	3.44 (4.64)
Ru/Al_2O_3	0.99 (0.31)	1.84 (0.59)
$Ru/CT/Al_2O_3$	0.80 (0.27)	1.33 (0.44)

[a] Obtained by means of back-extrapolation at zero pressure of the isotherm data in the 5–20 Torr range.

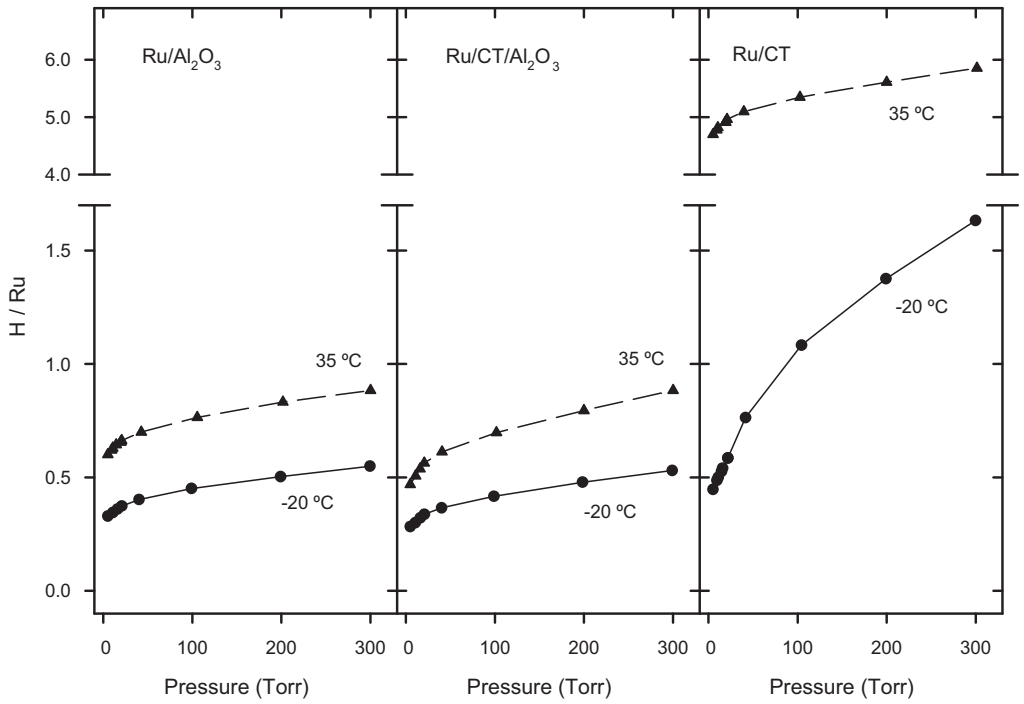

Fig. 9. H_2 adsorption isotherms obtained at −20 °C and 35 °C on the ruthenium catalysts. Volumetric adsorption data are shown in the form of apparent H/Ru ratio.

the methodology of H_2 volumetric experiences for obtaining metal dispersion data in ruthenium catalyst especially when there are significant hydrogen spill-over phenomena.

Table 4 summarizes the results of the CO volumetric chemisorption studies performed on the Ru catalysts. The interpretation of CO adsorption data over Ru supported onto alumina catalysts is quite complicated because there are several different CO species (linear, bridged and multicarbonyl) with diverse $CO/Ru_{surface}$ stoichiometry above and below one including both reduced and partially oxidized Ru sites [30]. Nevertheless we decided to measure the CO adsorption in order to obtain complementary data related to the metal dispersion of the catalysts. In this sense according to [31] the reversible (weak) CO chemisorption could involve both metal and support. Taking into account exclusively the amounts of CO irreversible adsorbed on the Ru/Al_2O_3 and $Ru/CT/Al_2O_3$ catalysts, the ruthenium dispersion must be higher in the former in good agreement with the H_2 chemisorption results.

In the case of the Ru/CT, the presence of a ceria-based mixed oxide makes even more complex the interpretation of the CO adsorption results as far as ceria reacts with CO forming carbonate species, their amount being related with its reduction degree [32]. In any case, the CO/Ru data obtained from irreversible chemisorption is significantly higher for this catalyst suggesting higher ruthenium dispersion with regard to the alumina containing samples.

Table 4
Volumetric studies of CO chemisorption on the Ru catalysts.

Catalyst	Amount of CO adsorbed in cm^3/g STP (CO/Ru)		
	Total[a]	Reversible[b]	Irreversible
Ru/CT	2.29 (1.54)	0.13 (0.09)	2.16 (1.45)
Ru/Al_2O_3	6.20 (0.99)	0.71 (0.11)	5.49 (0.88)
$Ru/CT/Al_2O_3$	3.64 (0.60)	0.35 (0.06)	3.29 (0.54)

[a] Obtained by means of the extrapolation at $P = 0$ of the first isotherm data in the 5–40 Torr pressure range.
[b] Obtained by means of the extrapolation at $P = 0$ of the second isotherm data in 5–40 Torr pressure range.

3.7. CO adsorption followed by means of FTIR spectroscopy

Fig. 10 shows the FTIR spectra of the catalysts treated with CO at r.t. in a wavenumber range where the CO species adsorbed on the Ru phase can be observed. The spectra for both alumina containing catalysts, Ru/Al_2O_3 and $Ru/CT/Al_2O_3$, are quite similar and consist of two bands (2125 and 2071 cm^{-1}) and a shoulder at 2002 cm^{-1}. Remarkably, the band at 2125 cm^{-1} does not appear on Ru/CT catalyst. In addition, the main band of CO adsorption over Ru/CT is around 2040 cm^{-1} with two small shoulders at 2110 and 1960 cm^{-1}. In spite of the well known complexity of the band assignment in ruthenium supported catalysts, in the case of

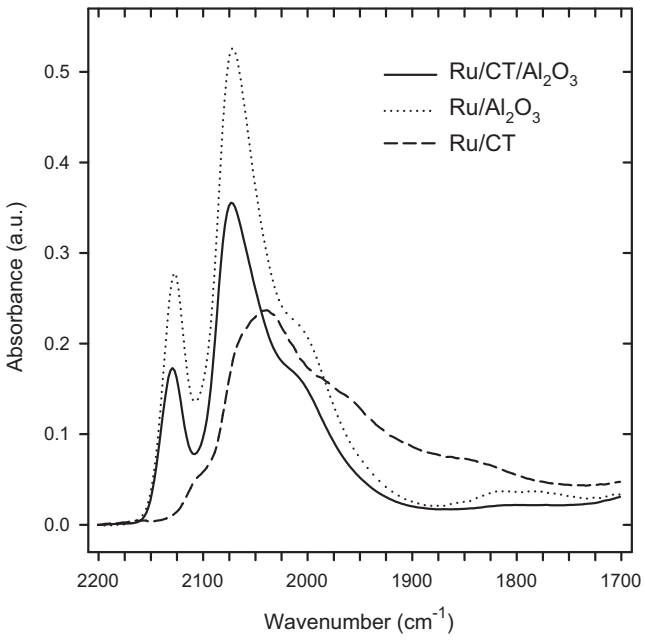

Fig. 10. FTIR spectra of CO adsorbed at r.t. on the ruthenium catalysts.

the Ru/Al_2O_3 the band at 2125 cm^{-1} can be attributed to the tricarbonyl CO species on Ru^{n+}, meanwhile the band at 2071 cm^{-1} and the shoulder at 2002 cm^{-1} are assigned to the di-carbonyl species adsorbed on Ru^{2+} [30]. Shifting band effects related to surface coverage and Ru crystallite size are not expected from this kind of ruthenium species [30,33]. These CO species adsorbed on positively charged Ru are not observed in the Ru/CT catalyst. According to the literature, the band at 2040 cm^{-1} in this catalyst must reasonably correspond to CO linearly adsorbed over Ru^0 as far as bands in the 1990–2060 cm^{-1} range have been attributed to these species being its exact position a function of the covering degree of the exposed ruthenium surface [33]. The shoulder at 1960 cm^{-1} and the low intense shoulder at 2110 cm^{-1} observed in the Ru/CT catalysts could be assigned to bridged CO on Ru^0 [30] and CO adsorbed on Ru^{n+} species [30,34], respectively. This clearly indicates that, depending on the support, Ru species with different electronic structure may coexist, those partially oxidized being stabilized by alumina in good accordance with [33]. Though the presence of Ru^0 in the ternary system cannot be discarded, most of the metal phase in $Ru/CT/Al_2O_3$ catalyst must be consequently more similar to that of Ru/Al_2O_3 than to the one existing in Ru/CT according to the FTIR results. This relationship between the samples resembles that observed in the catalytic study in relation with the temperature at which 50% of CO conversion is attained. On the contrary, the small fraction of Ru supported on the CT mixed oxide in the ternary system might explain its similarity with Ru/CT in relation with the capacity to full abatement of the unconverted CO via methanation, which is certainly the major catalytic feature. Obviously deeper research is needed to establish the role of the metal-support interaction in the activity of this kind of ruthenium catalysts for WGS and methanation reactions.

4. Concluding remarks

The work here presented is the preliminary study of a novel ternary catalyst consisting of Ru and a ceria–terbia mixed oxide (80/20 mol.%) prepared through sequential impregnation of an alumina support with the respective nitrate precursors of the promoter and metal phase. The aim of the study has been to obtain a system that may exhibit high activity in the water gas shift reaction with full CO abatement in a wide range of temperatures via simultaneous methanation of the unconverted carbon monoxide.

Taking into account the complexity of the $Ru/Ce_{0.8}Tb_{0.2}O_{2-x}/Al_2O_3$ catalyst here proposed special effort has been made in its characterization. In addition, $Ru/Ce_{0.8}Tb_{0.2}O_{2-x}$ and Ru/Al_2O_3 reference samples have been also investigated to better understand the ternary system properties and catalytic features.

The main conclusions of the characterization of the $Ru/Ce_{0.8}Tb_{0.2}O_{2-x}/Al_2O_3$ catalyst are the following:

1. The ceria–terbia mixed oxide is mainly present as solid solution in the form of aggregates consisting of particles of around 15 nm in size dispersed onto the alumina surface.
2. The ruthenium phase is also relatively well dispersed as particles with size in the range 1–4 nm corresponding to a dispersion around 40%. These particles are mainly located on the alumina as far as the promoter ceria–terbia mixed oxide is covering a relatively small fraction of the support surface.
3. We have found evidences of metal-support interaction phenomena affecting the electronic state of ruthenium. In particular, alumina favours Ru in ionic forms while Ru^0 species are mainly detected when this metal is supported on the ceria–terbia mixed oxide.

The main conclusion of the catalytic study carried out is that in both catalysts containing $Ru/Ce_{0.8}Tb_{0.2}O_{2-x}$ methanation reaction takes place along with WGS. Furthermore, the methanation occurs with high selective hydrogenation of CO in a CO_2 rich environment. As a consequence, in a region of temperatures where CO conversion should decrease according to thermodynamics full abatement of CO is reached with minimum consumption of hydrogen. In addition, the fact of including alumina as support of Ru and $Ce_{0.8}Tb_{0.2}O_{2-x}$ confers higher stability to the catalyst upon ageing under reaction conditions.

The overall results of this investigation suggest that the systems here proposed might be of interest for processes requiring high-pure hydrogen such as those related to fuel cell technology.

Acknowledgements

The authors thank the Ministry of Science and Innovation of Spain/FEDER Program of the EU (Project MAT2008-00889/NAN) and the Junta de Andalucía (FQM-110 group) for their financial support. X. Chen is grateful to Ramón y Cajal contract from Ministry of Science and Innovation, and Project FQM-3994 from Junta de Andalucía. We also acknowledge the SCCyT of Cadiz University (UCA) for using its electron microscopy division facilities.

Appendix A. Supplementary data

Supplementary data associated with this article can be found, in the online version, at doi:10.1016/j.cattod.2011.05.020.

References

[1] R. Farrauto, S. Hwang, L. Shore, W. Ruettinger, J. Lampert, T. Giroux, Y. Liu, O. Ilinich, Annu. Rev. Mater. Res. 33 (2003) 1.
[2] D.L. Trimm, Appl. Catal. A: Gen. 296 (2005) 1.
[3] J.R. Ladebeck, J.P. Wagner, in: W. Vilestich, H.A. Lamm (Eds.), Handbook of Fuel Cells, Fundamentals and Applications, Vol. 3, John Wiley & Sons, Chidchester, 2003, pp. 190–201, Part 2.
[4] R.J. Smith, M. Loganathan, M.S. Shantha, Int. J. Chem. React. Eng. 8 (2010) 1.
[5] G. Jacobs, B.H. Davis, Catalysis 20 (2007) 122.
[6] P. Kumar, R. Idem, Energy Fuels 21 (2007) 522.
[7] P. Djinovic, J. Batista, J. Levec, A. Pintar, Appl. Catal. A: Gen. 364 (2009) 156.
[8] E.B. Fox, S. Velu, M.H. Engelhard, Y. Chin, J.T. Miller, J. Kropf, C. Song, J. Catal. 260 (2008) 358.
[9] A. Goguet, R. Burch, Y. Chen, C. Hardacre, P. Hu, R.W. Joyner, F.C. Menunier, B.S. Mun, D. Thompsett, D. Tibiletti, J. Phys. Chem. C 111 (2007) 16927.
[10] L. Li, Y. Zhan, Q. Zheng, Y. Zheng, X. Lin, D. Li, J. Zhu, Catal. Lett. 118 (2007) 91.
[11] A.A. Fonseca, J.M. Fiher, D. Ozkaya, M.D. Shannon, D. Thompsett, Top. Catal. 44 (1–2) (2007) 223.
[12] M.A Hurtado-Juan, C.M.Y. Yeung, S.C. Tsang, Catal. Commun. 9 (2008) 1551.
[13] G. Jacobs, B.H. Davis, Appl. Catal. A: Gen. 284 (2005) 31.
[14] S. Bernal, G. Blanco, M.A. CAuqui, P. Corchado, J.M. Pintado, J.M. Rodríguez-Izquierdo, H. Vidal, Stud. Surf. Sci. Catal. 116 (1998) 611.
[15] T. Utaka, T. Okanishi, T. Takeguchi, R. Kikuchi, K. Eguchi, Appl. Catal. A: Gen. 245 (2003) 343.
[16] A. Basinska, T.P. Maniecki, W.K. Jozwiak, React. Kinet. Catal. Lett. 89 (2) (2006) 319.
[17] S. Bedrane, C. Descorme, D. Duprez, J. Mater. Chem. 12 (2002) 1563.
[18] D.P. VanderWiel, M. Pruski, T.S. King, J. Catal. 188 (1999) 186.
[19] M. Nawdali, H. Ahlafi, G.M. Pajonk, D. Bianchi, J. Mol. Catal. A: Chem. 162 (2000) 247.
[20] K.S.W. Sing, D.H. Everett, R.A.W. Haul, L. Moscou, R.A. Pierotti, J. Rouquerol, T. Siemieniewska, Pure Appl. Chem. 57 (4) (1985) 603.
[21] Y. Rozita, R. Brydsonl, A.J. Scottl, J. Phys.: Conf. Ser. 241 (2010) 1.
[22] G. Zhou, R.J. Gorte, J. Phys. Chem. B 112 (2008) 9869.
[23] J.Z. Shyu, W.H. Weber, H.S. Gandhi, J. Phys. Chem. 92 (1988) 4964.
[24] C. Bueno-Ferrer, S. Parres-Esclapez, D. Lozano-Castelló, A. Bueno-López, J. Rare Earths 28 (5) (2010) 647.
[25] S. Bernal, G. Blanco, G.A. Cifredo, J.J. Delgado, D. Finol, J.M. Gatica, J.M. Rodríguez-Izquierdo, H. Vidal, H. Hoser, Chem. Mater. 14 (2002) 844.
[26] S. Bernal, J.J. Calvino, M.A. Cauqui, J.M. Gatica, C. Larese, J.A. Pérez Omil, J.M. Pintado, Catal. Today 50 (1999) 175.
[27] J.M. Gatica, R.T. Baker, P. Fornasiero, S. Bernal, J. Kaspar, J. Phys. Chem. B (2001) 1191.
[28] J.G. Goodwin Jr., J. Catal. 68 (1981) 227.
[29] X. Shen, L.-J. Garces, Y. Ding, K. Laubernds, R.P. Zerger, M. Aindowa, E.J. Neth, S.L. Suib, Appl. Catal. A: Gen. 335 (2008) 187.

[30] S.Y. Chin, C.T. Williams, M.D. Amiridis, J. Phys. Chem. B 110 (2006) 871.
[31] C.H. Yang, J.G. Goodwin Jr., J. Catal. 78 (1982) 182.
[32] C. Binet, A. Badri, M. Boutonnet-Kizlingt, J.C. Lavalley, J. Chem. Soc. Faraday Trans. 90 (1994) 1023.
[33] C. Elmasides, D.L. Kondarides, W. Grünert, X.E. Verykios, J. Phys. Chem. B 103 (1999) 5227.
[34] J.A. De Los Reyes, M. Vrinat, M. Breysse, F. Maugé, J.C. Lavalley, Catal. Lett. 13 (1992) 213.